Disordering kinetics in monocrystalline and epitaxial Si upon energy deposition induced by dual-beam ion irradiation

Aurélien Debelle, G. Gutierrez, Alexandre Boulle, F. Garrido, O. Najjar, E. Olebunne, F. Pallier, C. Cabet, L. Thomé

Disordering kinetics in monocrystalline and epitaxial Si upon energy deposition induced by dual-beam ion irradiation

A. Debelle[1,2], G. Gutierrez[2], A. Boulle[3], F. Garrido[1], O. Najjar[1,4], E. Olebunne[1], F. Pallier[1], C. Cabet[2], L. Thomé[1]

[1]Université Paris-Saclay, CNRS/IN2P3, IJCLab, 91405 Orsay, France.

[2]Université Paris-Saclay, CEA, Service de Recherches de Métallurgie Physique, 91191 Gif-sur-Yvette, France

[3]IRCER, CNRS UMR 7315, Centre Européen de la Céramique, 12 rue Atlantis, 87068 Limoges Cedex, France

[4]An Najah National University, Civil Engineering department, Omar Ibn Al-Khattab St, Nablus, West Bank, Palestine

Abstract

In this work, the effect on the amorphization process of the simultaneous electronic (S_e) and nuclear (S_n) energy deposition occurring upon dual-beam irradiation experiments was studied in both bulk Si single crystals (Si-b) and epitaxial Si thin layers (Si-tl). For this purpose, 900 keV I (for S_n) and 27 MeV Fe (for S_e) ions were used at different fluences in order to get complete disordering kinetics. These later were determined through the monitoring of both the disorder fraction, obtained via Rutherford backscattering spectrometry in channeling experiments and the elastic strain derived from X-ray diffraction measurements. Raman 2D-maps were also recorded to support the results of the two other techniques. RBS/C data indicate that S_n irradiation alone leads to full amorphization of the irradiated region in both Si-b and Si-tl at a fluence of 1.5×10^{14} cm^{-2}. In contrast, during the dual-beam irradiation (S_n&S_e), such a complete phase transformation is prevented up to a fluence of 3×10^{14} cm^{-2}. Similarly, the maximum elastic strain developing before the loss of crystallinity reaches a maximum of ~1 % at 1.5×10^{14} cm^{-2}, but it remains below 0.2 % at the same fluence in the S_n&S_e regime for which full amorphization is not detected. These results indicate that the electronic energy deposition induces a significant dynamic annealing of the damage created by the nuclear energy-loss, and this annealing occurs over the entire investigated fluence range (i.e. up to 3×10^{14} cm^{-2}). The annealing efficiency is shown to be lower for Si-tl, as demonstrated by the disorder and strain values that are always larger than for the bulk counterpart.

I – Introduction

The late 20th century to early 21st century has been described as the Silicon Age, for this element represents the key (semiconductor) material in microelectronics [1-3]. In its bulk form, or as a thin layer deposited onto an insulator (so-called silicon on insulator, SOI) [4], it is mainly used to create a PN junction which constitutes the building brick of transistors, diodes, integrated circuits and so on. Those elements are then used to design ever increasingly complex electronic devices. Therefore, Si-based materials are found in various fields of physics and materials science that include, to cite just a few, central processing units, energetic particle detectors (for instance in large-scale accelerator facilities) [5-6], sensors for space applications [7], photovoltaic cells [8] and lithium batteries [9-10]. For most of these uses, and also for functional design at the nanoscale such as nanobubble formation [11] or doping [1,12], silicon is subjected to ion irradiation, an operation during which complex energy deposition processes are involved. These latter may lead to intricate modifications of the material microstructure and can potentially have detrimental effects on its physical properties.

The slowing-down of a charged particle with a low velocity (as compared to the root-mean square velocity of its own electrons) passing through matter can be essentially described by elastic (so-called nuclear or ballistic) collisions between the projectile and the screened nuclei of the target atoms. During this type of interactions, part of the projectile kinetic energy is transferred to target atoms. If this transferred energy is larger than a threshold displacement energy (E_d), the primary knock-on atom is ejected with a velocity sufficient to induce collective displacements of target atoms; this phenomenon is referred to as a collision cascade [13] and the associated slowing-down process is called nuclear stopping power (S_n). Swift charged particles essentially interact with electrons of the target atoms, which leads to excitations and ionizations, and this slowing-down is usually referred to as electronic stopping power(S_e). Yet, via an electron-phonon coupling, a significant amount of the deposited energy can reach the atomic network, which may produce atomic displacements [13]. Understanding the energy partitioning between the electronic and atomic networks constitutes an important issue to tackle, and it currently represents a hot topic, as demonstrated by a recent review paper on that very subject (see [14] and references therein). One reason for this interest lies in the fact that combined - hereafter denoted as $S_n\&S_e$ - effects can take place and these latter are not necessarily additive. In that case, they are frequently referred to as *synergistic*

effects (i.e. the result is not the algebraic sum of the different contributions). A comprehensive description and understanding of these complex phenomena can help designing materials for tailored properties [13-14]. One way to address this subject is to perform dual-beam irradiation experiments in order to have both, selected S_n and S_e components (another option consists in using tens of MeV ions for which both components are present).

It is not in the scope of this paper to provide a review of irradiation-induced disordering or annealing effects in Si (the reader can refer to review papers for that purpose [15-16]). Here, we will only recall that Si is highly sensitive to nuclear collisions and undergoes amorphization when irradiated at room temperature (RT) at a fraction of displacement per atom (dpa). In contrast, Si is particularly resistant against ionizing events occurring with high-velocity ions [17] (one of the reasons why it is used to detect high-energy particles [18]). Both low- [15] and high-velocity [19] ions can be used to induce recrystallization of amorphous Si layers at temperatures around 200-400°C. This phenomenon is referred to as the (swift-heavy) ion-beam-induced epitaxial crystallization (SH-IBIEC) phenomenon [15,16,19]. Recently, we even demonstrated that disorder annealing can occur during dual-beam irradiation [20]. More precisely, a substantial quantity of defects generated by nuclear collisions (S_n) are eliminated by the deposited electronic energy of swift ions (S_e). This phenomenon (referred to as SNEEL, which stands for synergy between nuclear and electronic energy-losses) does take place in Si [21]. We showed that its magnitude increases with the flux ratio between the S_e- and the S_n-beam. In that study, we investigated only the final stage of the amorphisation process, i.e. we used samples irradiated at fluences that would normally lead to full amorphization. In the present paper, we provide complete, quantitative disordering kinetics (under S_n and S_n&S_e irradiations); in addition, we compare bulk Si and Si thin layers deposited onto an oxide substrate.

II - Experimental

The samples used in this study are n-type {100}-oriented Si single crystals with a thickness of 280 µm provided by Neyco (hereafter referred to as Si-b), and Si layers with a thickness of about 500 nm deposited onto a sapphire (Al_2O_3) substrate provided by MTI Corporation (hereafter referred to as Si-tl).

Si-b and Si-tl were irradiated together at RT at the JANNuS-Saclay facility [22] with either a single 900 keV I ion beam (hereafter referred to as S_n) or a dual beam of 900 keV I and 27 MeV Fe ions (hereafter referred to as S_n&S_e). The ion fluences were increased up to $3x10^{14}$ cm^{-2} for I and $5.4x10^{14}$ cm^{-2} for Fe; the ratio between S_e and S_n ion fluxes was 1.8 in order to maximize the synergy effect [20]). The irradiation temperature was monitored with thermocouples and with a thermal imaging camera. Simulations of the ion/silicon interactions were performed with the SRIM2011 code in full damage cascades mode [23], using a threshold displacement energy of 20 eV [24]. These results are presented and commented in section III.1.

Rutherford backscattering spectrometry in channeling condition (RBS/C) was performed using a 1.4 MeV He ion beam delivered by the ARAMIS accelerator of the JANNuS-SCALP platform at IJClab in Orsay [22]. Experimental spectra were fitted using the McChasy Monte-Carlo code developed at the National Centre for Nuclear Research (NCBJ) in Warsaw [25], with the assumption that a fraction of atoms, f_D, are randomly displaced from their regular crystallographic site.

High-resolution X-ray diffraction characterizations were carried out on a Bruker D8 Discover at IRCER in Limoges. A parallel and monochromatic (λ=0.15406 nm) incident X-ray beam was used to probe the 004 Bragg reflection performing so-called θ-2θ scans. Experimental data were fitted with the computer code named RaDMaX-Online [26-27]. From these simulations, elastic-strain depth profiles were determined in the irradiated samples.

Raman characterizations with a frequency-doubled Nd:YAG (532 nm) laser and a 2400 groove/mm grating were performed for pristine and irradiated samples using an Invia Reflex Renishaw spectrometer coupled to a Leica microscope with a 100x objective. A laser power lower than 0.05 mW was used in order to avoid sample modifications during measurements. The Raman spectrometer was calibrated by using standard silicon monocrystalline samples.

III – Results

III.1. SRIM results

Figure 1 presents the S_n and S_e depth profiles of both 900 keV and 27 MeV Fe ions. Only the first µm is shown because this thickness fully encompasses the region perturbed by I ions, and this work focuses on the evolution of this very region upon sole S_n or dual S_n&S_e irradiations. In this region, the S_n component of 900 keV I ions, referred to as $S_n(I)$, peaks at 2 keV/nm, which is high enough to induce a significant disorder, as shown in, e.g. [16, 21, 29] and hereafter. In contrast, $S_e(I)$ is below 1 keV/nm, which is far below the threshold level (~37 keV/nm) for significant disordering in Si [17]. $S_n(Fe)$, which is about 0.1 keV/nm in the first µm, can be neglected in terms of damage creation, as shown in the Supplementary Information (SI) file that presents the RBS/C results for the sole 27 MeV irradiation (Fig. S1), and as reported in [32] with similar ions (23 MeV I). Note that $S_n(Fe)$ is more significant at the end-of-range of the 27 MeV Fe ions, and at this depth, it does induce disorder, not visible by RBS/C (Fig.S1), but obvious in the Raman cross-section provided in the SI file (see Fig. S2). In contrast, $S_e(Fe)$ is ~5.5 keV/nm, a level sufficient to induce defect annealing, as previously reported by the authors in [21], and as further demonstrated hereafter. In summary, the present work considers that only $S_n(I)$ creates disorder and $S_e(Fe)$ partially heals this disorder.

III.2. RBS/C

Figure 2 (a,b) presents raw and simulated RBS/C data for Si-b and Si-tl irradiated either with a single 900 keV I ion beam (Fig. 2a) or simultaneously with a dual 900 keV I and 27 MeV Fe ion beam (Fig. 2b). Figure 2 (c,d) presents the damage fractions (f_D) extracted from McChasy simulations of RBS/C spectra plotted in Figure 2 (a,b). Data recorded in the case of single I ion irradiation (Fig. 2 a,c) exhibit the presence of a damage peak at a depth of ~250 nm, with a magnitude that increases with the I fluence, for both Si-b and Si-tl. This peak reaches the random level (f_D=1) at a fluence of 1.5×10^{14} cm^{-2}, suggesting that the samples are amorphized at 250 nm at (and above) this fluence. The amorphous layer expands towards both the surface and greater depth as the I fluence is further increased (3×10^{14} cm^{-2}). It is worth mentioning that pristine Si layers are intrinsically slightly defective (because of epitaxial growth defects) and are thus characterized by an initial disorder level higher than that of bulk Si crystals, as indicated by the RBS/C spectra recorded on these samples (compare curves labelled ‘virgin’ in Fig. 2a).

Data recorded in the case of dual I and Fe ion irradiation (Fig. 2 b,d) show less defective crystals at similar I fluences than in the case of I irradiation alone, and for the two types of materials. Moreover, amorphization of both Si-b and Si-tl is prevented at 1.5×10^{14} cm^{-2} and even at 3×10^{14} cm^{-2} (f_D is lower than 1 all over the irradiated region). These results confirm that a synergistic effect takes place in bulk Si irradiated with a dual low- and high-energy ion beam (see Ref. [21]), and they show that this effect also occurs in Si layers.

III.3. XRD

Figure 3 presents XRD data for irradiated Si-b (Fig.3 a,c) and Si-tl (Fig.3 b,d). Only XRD curves for which full amorphization was not achieved (as estimated by this technique) are displayed in this figure. Full amorphization was assumed when the scattered intensity became extremely low. An exception was made for some samples where a severely disordered, but still crystalline region at the backside of the amorphized layer was present, allowing an acceptable fit. In Figure 3a, XRD results corresponding to Si-b irradiated with 900 keV I (S_n) are shown. Such type of XRD signal has been extensively described elsewhere [26-28]. The fringe pattern at low scattering angle indicates the presence of a tensile strain depth profile. This latter can be retrieved by simulating the experimental data (see black solid lines in Fig. 3a), and the corresponding profiles are displayed in the inset of Fig. 3a. It can be noted that both the shape and the depth extension of the strain profiles are in agreement with those of the disorder distributions determined by RBS/C (Fig. 2c), meaning that both techniques provide consistent results. The strain level increases with increasing I fluence, until full amorphization (with the viewpoint of this technique) takes place at 1.5×10^{14} cm^{-2} over 280 nm; this is the reason why the corresponding strain profile is truncated from the surface until this depth. Figure 3b shows XRD data of I-irradiated Si-tl. The corresponding signals consist in single, broad peaks (because of a thin damaged layer), with a huge asymmetry on the low-angle side. The right-side component comes from the remaining pristine layer (because the total layer thickness is slightly larger than the damaged thickness), while the left-side component is due to the irradiated, strained part of the layers. Hence, a tensile strain developed in these layers, similar to what happened in the bulk samples (note that the position of the Bragg peak for the pristine layers is not that for the single-crystals because the layers exhibit an intrinsic – epitaxial – strain due to the lattice misfit between the Si layer and the sapphire substrate). Corresponding strain profiles are displayed in the inset of Figure 3b. These profiles (i.e.,

overall, bell-shape-like profiles) are similar to those found for bulk Si and thus, they also agree with the f_D profiles determined by RBS/C.

In Fig. 3 (c,d) are plotted similar data as in Fig. 3(a,b) but for dual-beam (S_n&S_e) irradiated materials. The abscissae are identical to those used for the single-beam irradiation. It can hence be readily observed that the signal extension or shift towards low angles is much less pronounced for S_n&S_e irradiation than it is for S_n irradiation alone. This finding indicates that the strain developing during the I&Fe irradiation exhibits a lower level than that measured for I irradiation alone. Strain profiles are displayed in the insets of Figure 3 (c,d). They globally exhibit a shape similar to that of the sole S_n irradiation, but the strain magnitude is much lower. Importantly, it was possible to determine the strain level up to higher fluences, i.e. 1.5x10^{14} cm^{-2} (for S_n&S_e) *vs* 9x10^{13} cm^{-2} (for S_n) in the case of Si-b.

III.4. Raman

Figure 4 shows typical Raman data recorded on pristine and ion-irradiated silicon. The pristine spectrum (Fig. 4a) exhibits the characteristic Raman mode of crystalline silicon: a longitudinal optical (LO) phonon band at 520 cm^{-1} (c-Si). When a Si crystal is amorphized, the c-Si peak disappears and a broad peak, centred at 480 cm^{-1} (a-Si), is observed. In the case of single I ion irradiation (S_n), the spectrum recorded at the sample surface (Fig. 4a) exhibits the presence of both c-Si and a-Si peaks. On the contrary, in the case of dual I and Fe ion irradiation (S_e), only the c-Si peak is observed. Figure 4(b,c) presents the 2D Raman intensity distribution (so-called 2D maps) obtained by recording Raman spectra on a cross-section sample as a function of the depth along the I and Fe ion path. Figure 4b corresponds to Si-b irradiated with 900 keV I ions and Fig. 4c to Si-b irradiated with a dual 900 keV I and 27 MeV Fe ion beam; in both cases, the same 3x10^{14} cm^{-2} iodine fluence was used. The Raman signal was recorded over 0.7 µm for each sampling depth point performed every 0.1 µm. Each spectrum of the map is thus the result of the intensity integrated over the laser spot surface. As the damaged depth is smaller than the laser spot size, a signal coming from both the damaged and the pristine parts is always measured. In Fig. 4b, i.e. for the S_n irradiation alone, the intensity of the a-Si peak is intense up to a depth of ~350 nm, whereas only the c-Si peak is observed for the S_n&S_e irradiation (Fig. 4c). For the S_n irradiation, the concomitant presence of a-Si and c-Si peaks between 0 and 400 nm can be explained by the laser spot size (0.7 µm). It can be noted that the depth extension of the Raman map is in good agreement with the disorder

distribution determined by RBS/C (Fig. 2c), which indicates consistent results between the two techniques.

IV – Discussion

Using three different techniques, namely RBS/C, XRD and Raman, it has been shown that the electronic energy deposition (S_e) due to 27 MeV Fe ions significantly reduces the disorder created by ballistic collisions (S_n) induced by 900 keV I ions when both ion beams are used simultaneously. Hereafter, for a more quantitative description of this effect, we plot the variation of the disorder determined by RBS/C and of the elastic strain derived from XRD as a function of the iodine fluence; these curves are called disordering kinetics.

Figure 5 presents the disordering kinetics obtained from the RBS/C data shown in Figure 2 (i.e. f_D as a function of the I ion fluence). Note that, in this figure, f_D represents the peak damage measured at around 250-300 nm (for some thin layers where there is no identifiable peak, the disorder was also taken in this depth region). Note also that the intrinsic disorder component in the thin layers has been subtracted to the disorder determined in the irradiated layers. Yet, the results show that f_D for Si-tl is always higher than f_D for Si-b at the same ion fluence. This feature should be related to the fact that the pristine layers exhibit an intrinsic disorder that is much more pronounced than their bulk counterparts, and this initial disorder may accelerate the disordering process upon irradiation. In the case of I ion irradiation alone, f_D increases monotonously but exhibits a sharp rise above ~7×10^{13} cm^{-2} for both Si-b and Si-tl samples; it reaches a value of 1 at 1.5×10^{14} cm^{-2}, meaning that full amorphization occurred at this fluence. As reviewed in [15], and later modelled in an original way by Edmondson et al. [29], amorphization in Si should in fact, upon the current conditions, be heterogeneous, i.e. it proceeds from a multi-step process. In the current work, the variation of f_D can indeed be described by a two-step mechanism, similarly to what was done for ion-irradiated SiC [30] using a dedicated (called MSDA) model [31]. The fitting result is displayed as a solid blue line in Figure 5 (note that, for clarity purposes, and because the fit was only made for a qualitative description, both sets of data, i.e. Si-b and Si-tl, were fitted together).

The disordering kinetics in the case of dual I and Fe ion irradiation are different from those observed for the sole I irradiation, in the sense that the disorder level is significantly lowered over the entire investigated fluence range for both Si-b and Si-tl. Therefore, even at the highest investigated fluence, f_D never reaches unity upon $S_e\&S_n$ irradiation, indicating that amorphization was never completed. It is important to mention, that, even though the

maximum disorder is found to be 0.8, a substantial damage annealing did occur, as evidenced by the profiles shown in Fig.2 (c, d). Another evidence of this annealing can be provided looking at the disorder level at the I fluence of $9x10^{13}$ cm^{-2}: it is 0.8 after the sole I irradiation, while it does not exceed 0.2 after the dual-beam experiment, which is a significant decrease. Such a very similar reduction in the disorder level has been very recently observed in silicon submitted to 23 MeV I irradiation subsequent to 600 keV I irradiation [32].

Qualitatively, the overall shape of the disordering curves is yet similar to the one observed upon S_n irradiation; in particular, the two-step mechanism is still present, although the disordering rate for each step is significantly lowered. It is however important to mention that the f_D parameter does not take into account the defect nature, which prevents any firm interpretation of a possible change in the amorphization mechanism. For instance, in bulk Si, it was shown that a different microstructure develops upon dual-beam irradiation as compared to single low-energy irradiation [21]. The thermal energy brought to the system by the electronic energy deposition is supposed to enhance the defect mobility, which leads to both defect reorganization (i.e. new defects, such as dislocations) and recombination. Hence, the disordering process may be different upon the two beam conditions, but a detailed microscopy analysis is required to provide a definitive conclusion. Finally, it is worth mentioning that the disordering rate is higher in Si-tl than it is in Si-b, which suggests that the initial disorder in the layers not only affects the amorphization process upon the sole S_n irradiation, but it also decreases the annealing efficiency of the electronic energy deposition process. A similar result was provided in the early 1980's by Svensson et al. who compared the recrystallization taking place in pre-damaged bulk Si and in silicon on sapphire layers submitted to elastic energy deposition at 200 and 300 °C [33]. Although the annealing mechanism was not similar to the one involved in the current work (IBIEC vs SNEEL), two conclusions that may also hold here were drawn: pre-existing defects in thin layers seem to be highly stable and cannot be annealed upon (any type of) ion irradiation, and those defects most likely stabilize part of the irradiation-induced defects.

Figure 6 presents the strain buildups extracted from the XRD data of Figure 3, where the maximum strain of the profiles shown in Figure 3 is plotted as a function of the I fluence (note that the intrinsic epitaxial strain component in the thin layers has been subtracted to the measured strain). Regarding S_n irradiations, the results show that both Si-b and Si-tl exhibit an overall similar behavior (but noticeable differences exist, as discussed hereafter). For both

types of materials, the strain increases almost linearly with the I fluence in a first stage, i.e. up to ~7x10^{13} cm^{-2}. This finding is in agreement with the results of a seminal paper on the strain developing during the irradiation-induced amorphization process in Si [34]. It is worth mentioning that this fluence corresponds to the one for which the disorder determined by RBS/C dramatically increases (i.e., the beginning of the second step of the amorphization process). Above this fluence, the Si layers are too defective for the strain to be determined; however, for the single-crystals, a maximum strain of ~1 % can still be measured at 9x10^{13} cm^{-2}. Besides, an increase of the strain rate is noticed between 7x10^{13} cm^{-2}and 9x10^{13} cm^{-2}. These results are in agreement with previous works that showed a similar multi-step strain buildup (with values very close to those currently measured) in irradiated Si single-crystals [34-35]. Regarding bulk Si versus Si on thin layer, there exists two major differences: the smaller fluence range for which Si layers remains partially crystalline, and the higher strain levels that they systematically exhibit. Thus, the current XRD results tend to indicate that the intrinsic disorder in the thin layers increases the strain rate.

For S_n&S_e irradiations, strain develops in both types of materials, but the strain rate is significantly decreased as compared to the case of sole S_n irradiations. Moreover, the strain can be determined up to the fluence of 1.5x10^{14} cm^{-2} for both Si-b and Si-tl, because the crystalline lattice is less severely damaged than in the case of the S_n irradiations alone. Consequently, the strain levels are systematically lower, i.e., for instance, less than 0.2 % at 9x10^{13} cm^{-2} for Si-b irradiated upon S_e&S_n as compared to ~1 % at the same fluence upon S_n. At the same fluence, for Si-tl, the maximum strain measured upon S_e&S_n is lower than 0.4 %, while it was already not anymore measurable during the S_n *i*rradiation only. These quantitative results provide additional support of (i) the annealing process occurring upon dual-beam irradiation, and of (ii) the lower efficiency of this process in the thin layers as compared to the single-crystals. The consequence of this dynamic annealing is an increased fluence range over which the (silicon) crystalline structure is maintained, as illustrated in both Figures 5 and 6.

.

Conclusion

The amorphization process of Si exposed to ion irradiation was investigated in two cases: (i) using 900 keV I for which the nuclear energy loss (S_n) is dominant, and (ii) with a dual-beam, i.e. 900 keV I and 27 MeV Fe, designed to lead to concomitant electronic (S_e) and nuclear energy depositions. Both bulk Si single crystals (Si-b) and epitaxial Si thin layers (Si-tl) deposited onto sapphire were studied using RBS/C, XRD and Raman techniques. Only the first µm was studied, which is the region where I ions generate disorder. The elastic strain and the disorder fraction were determined in this region as a function of the I fluence. One major, dramatic difference was observed between the disordering kinetics determined for S_n irradiation alone on the one hand, and coupled S_n&S_e experiments on the other hand: while full amorphization was reached at the damage peak at 1.5×10^{14} cm^{-2} in the former case, a partially crystalline lattice was still present at 3×10^{14} cm^{-2} in the latter case. In fact, the disordering rate was significantly reduced upon S_n&S_e irradiation over the entire investigated fluence range. The strain developing in the S_n-irradiated region is also considerably reduced (more than twice), in agreement with a lower disorder fraction, and thus with a lower defect density. The electronic energy deposition (S_e) allows part of the defects generated during elastic collisions (S_n) to be annealed. However, the intrinsic defects present in the epitaxial layers are stable against this energy deposition, and they seem to both increase the disordering rate and decrease the annealing efficiency. This work provides useful data as Si (either in its bulk form or as a thin layer) is widely used as a material for radiation-harsh applications.

Acknowledgments

We acknowledge the French EMIR-A network for providing irradiation beamtime and we grant the JANNuS-Saclay staff for their efficiency in performing the irradiation experiments. We also thank the JANNuS-SCALP platform staff for their help during the RBS/C measurements.

Conflict of interest

Authors declare no conflict of interest at all.

Supplementary Information

Below is the link to the electronic supplementary material.

References

[1] Hull R (1999) Properties of crystalline silicon, ed. Univ. Virginia, INSPEC, London.

[2] Thompson S.E, Parthasarathy S (2006) Moore's law: the future of Si microelectronics, Materials Today 9:20-25.

[3] Venema L Silicon (2011) Electronics and Beyond Nature Insight 479:309-353.

[4] Nguyen B Y, Celler G, Mazuré C (2009) A review of SOI technology and its applications Journal Integrated Circuits and Systems 4:51-54.

[5] P J Dervan (2012) Silicon strip detectors for the ATLAS HL-LHC upgrade Journal of Instrumentation 7:C03019.

[6] Moll M (2018) Displacement Damage in Silicon Detectors for High Energy Physics IEEE Trans. Nucl. Science 65:1561-1582.

[7] Morselli A (2008) Silicon detectors in space for γ-ray astroparticle physics Nucl. Instr. Methods A 596:79-84.

[8] Hall R N (1981) Silicon photovoltaic cells Solid-State Electronics 24:595-616.

[9] Dimov N, Xia Y, Yoshio M (2007) Practical silicon-based composite anodes for lithium-ion batteries: fundamental and technological features J. Power Sources 171:886-893.

[10] McGehee W R, Strelcov E, Oleshko V P, Soles C, Zhitenev N B, McClelland J J (2019) Direct-Write Lithiation of Silicon Using a Focused Ion Beam of Li^+ ACS Nano 13: 8012-8022.

[11] Maleville C, Aspar B, Poumeyrol T, Moriceau H, Bruel M, Auberton-Herve A.J, Bargen T (1997) Wafer bonding and H-implantation mechanisms involved in the Smart-cut technology, Mater. Sci. Eng. B 46:14-19.

[12] Manchester K E, Sibley C B, Alton G (1965) Doping of silicon by ion implantation Nucl. Instr. Methods 38:169-174.

[13] Wesch W, Schnohr C.S (2016) Ion Beam Modification of Solids, chap. 9, ed Springer International Publishing, Switzerland.

[14] Zhang Y, Weber W J (2020) Ion irradiation and modification: The role of coupled electronic and nuclear energy dissipation and subsequent nonequilibrium processes in materials Appl. Phys. Rev. 7:041307.

[15] Priolo F., Rimini E. (1990) Ion-beam-induced epitaxial crystallization and amorphization in silicon Materials Science Report 5:319-379.

[16] Pelaz L, Marqués L A, Barbolla J (2004) Ion-beam-induced amorphization and recrystallization in silicon J. Appl. Phys. 96:5947-5958.

[17] Kamarou A, Wesch W, Wendler E, Undisz A, Rettenmayr M (2008) Radiation damage formation in InP, InSb, GaAs, GaP, Ge, and Si due to fast ions Phys. Rev. B. 78:054111.

[18] Allport P (2019) Applications of silicon strip and pixel-based particle tracking detectors Nature Reviews Physics 1:567-576.

[19] Sahoo P K, Som T, Kanjilal D, Kulkarni V N (2005) Swift heavy ion beam induced recrystallization of amorphous Si layers NIM B 240:239-244.

[20] Thomé L, Debelle A, Garrido F, Trocellier P, Serruys Y, Velisa G, Miro S (2013) Combined effects of nuclear and electronic energy losses in solids irradiated with a dual-ion beam Appl. Phys. Lett. 102:141906.

[21] Thomé L, Gutierrez G, Monnet I, Garrido F, Debelle A (2020) Ionization-induced annealing in silicon upon dual-beam irradiation J. Mater. Sci. 55:5938-5947.

[22] Gentils A, Cabet C (2019) Investigating radiation damage in nuclear energy materials using JANNuS multiple ion beams Nucl. Instr. Meth. B 447:107-112.

[23] Ziegler J F, Biersack J P, Littmark U (1985) The Stopping and Range of Ions in Solids, Pergamon, New York, available at: www.srim.org.

[24] Holmström E, Kuronen A, Nordlund K (2008) Threshold defect production in silicon determined by density functional theory molecular dynamics simulations Phys. Rev. B 78:045202.

[25] Nowicki L, Turos A, Ratajczak R, Stonert A, Garrido F (2005) Modern analysis of ion channeling data by Monte Carlo simulations Nucl. Instr. Meth. B 240:277-282.

[26] Souilah M, Boulle A, Debelle A (2016) RaDMaX: a graphical program for the determination of strain and damage profiles in irradiated crystals J. Appl. Cryst. 49:311-316.

[27] Boulle A, Mergnac V (2020) RaDMaX online: a web-based program for the determination of strain and damage profiles in irradiated crystals using X-ray diffraction J. Appl. Cryst. 53:587-593.

[28] Debelle A, Declémy A (2010) XRD investigation of the strain/stress state of ion-irradiated crystals Nucl. Instr. and Methods B 268:1460-1465.

[29] Edmondson P D, Riley D J, Birtcher R C, Donnelly S E (2009) Amorphization of crystalline Si due to heavy and light ion irradiation J. Appl. Phys. 106:043505.

[30] Debelle A, Thomé L, Dompoint D, Boulle A, Garrido F, Jagielski J, Chaussende D (2010) Characterization and modelling of the ion-irradiation induced disorder in 6H-SiC and 3C-SiC single crystals J. Phys. D: Appl. Phys. 43:455408.

[31] Jagielski J, Thomé L (2011) Multi-step damage accumulation in irradiated crystals Applied Physics A 97:147-155.
[32] Tomic Luketic K, Karlušic M, Gajovic A, Fazinic S, O'Connell J H, Pielic B, Radatovic B, Kralj M (2021) Investigation of Ion Irradiation Effects in Silicon and Graphite Produced by 23 MeV I Beam Materials 14:1904.
[33] Svenson B, Linnros J, Holmén G (1983) Ion-beam induced annealing of radiation damage in silicon on sapphire Nuclear Instruments and Methods 209/210:755-760.
[34] Speriosu V S, Paine B M, Nicolet M A, Glass H L (1982) X-ray rocking curve study of Si-implanted GaAs, Si, and Ge Appl. Phys. Lett. 40:604.
[35] Bai G, Nicolet M A (1991) Defects production and annealing in self-implanted Si Journal of Applied Physics 70:649-655.

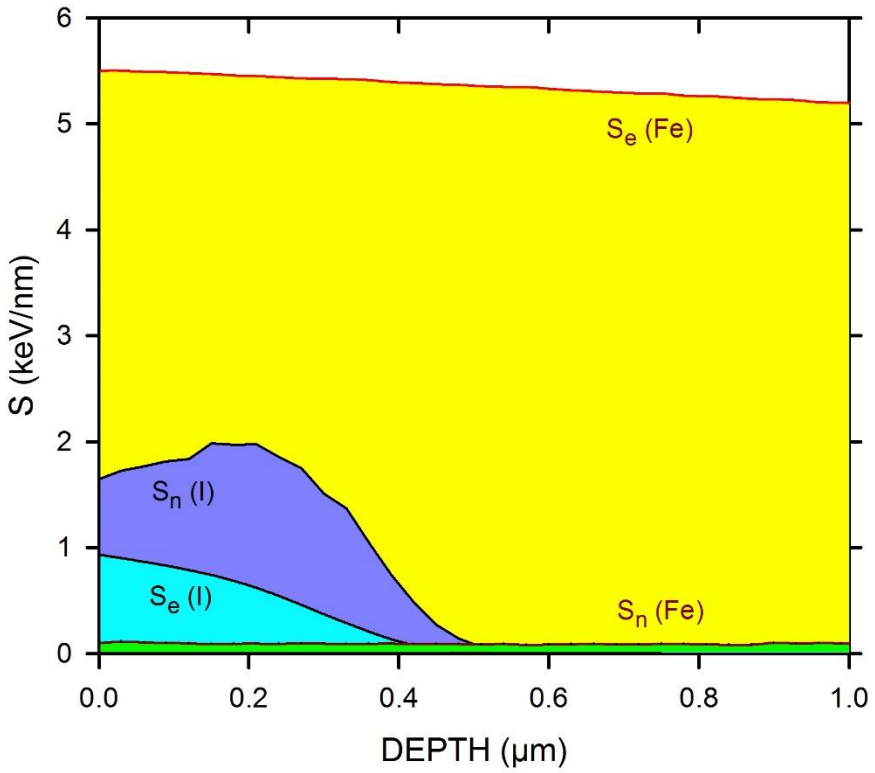

Figure 1

Nuclear (S_n) and electronic (S_e) energy losses *vs* depth for Si irradiated with low-energy I ions (blue and cyan areas, respectively) and high-energy Fe ions (green and yellow areas, respectively). Calculations were performed with the SRIM2011 code [23].

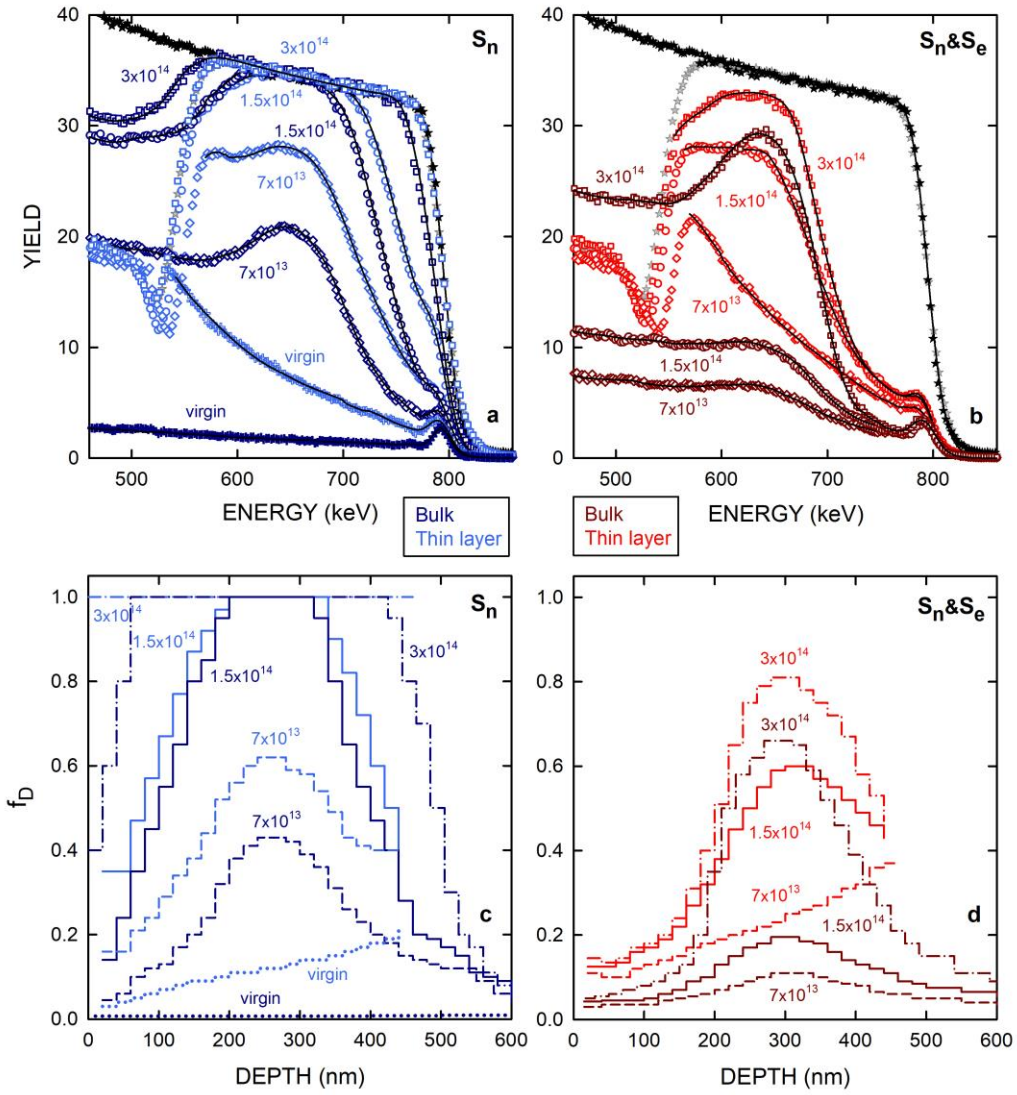

Figure 2

(a,b) RBS spectra (Si signal) recorded along random (Si-b, black stars and Si-tl, grey stars) and <001> axial (other symbols) directions on Si-b (dark-blue and dark-red symbols) and Si-tl (light-blue and light-red symbols) irradiated at RT with 900 keV I ions (a) or with 900 keV I ions and 27 MeV Fe ions (b). The numbers are the I fluences (in cm^{-2}) used for both S_n and S_n&S_e irradiations. Solid lines are best fits to experimental data using the McChasy code [25].

(c,d) Damage fraction (f_D) as a function of depth, extracted from the fits to experimental RBS/C data of Fig. 2 (a,b), for Si-b (dark-blue and dark-red lines) and Si-tl (light-blue and light-red lines) irradiated at RT with 900 keV I ions (c) or with 900 keV I ions and 27 MeV Fe ions (d).

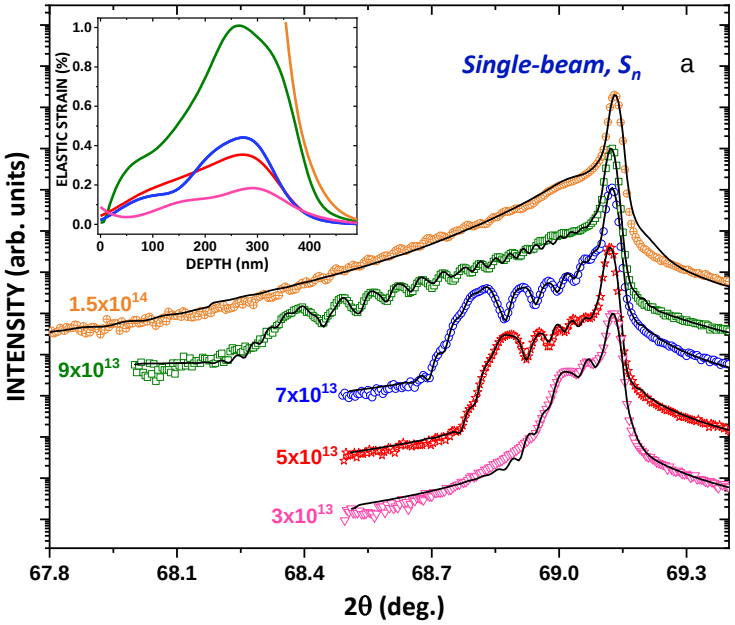
Single-beam, S_n
a
INTENSITY (arb. units)
2θ (deg.)
ELASTIC STRAIN (%)
DEPTH (nm)
1.5x10^14
9x10^13
7x10^13
5x10^13
3x10^13

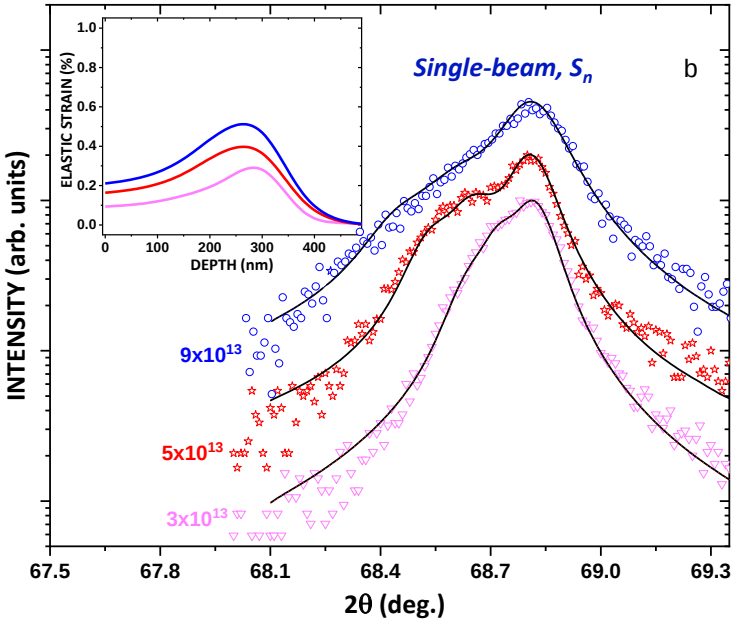
Single-beam, S_n
b
INTENSITY (arb. units)
2θ (deg.)
ELASTIC STRAIN (%)
DEPTH (nm)
9x10^13
5x10^13
3x10^13

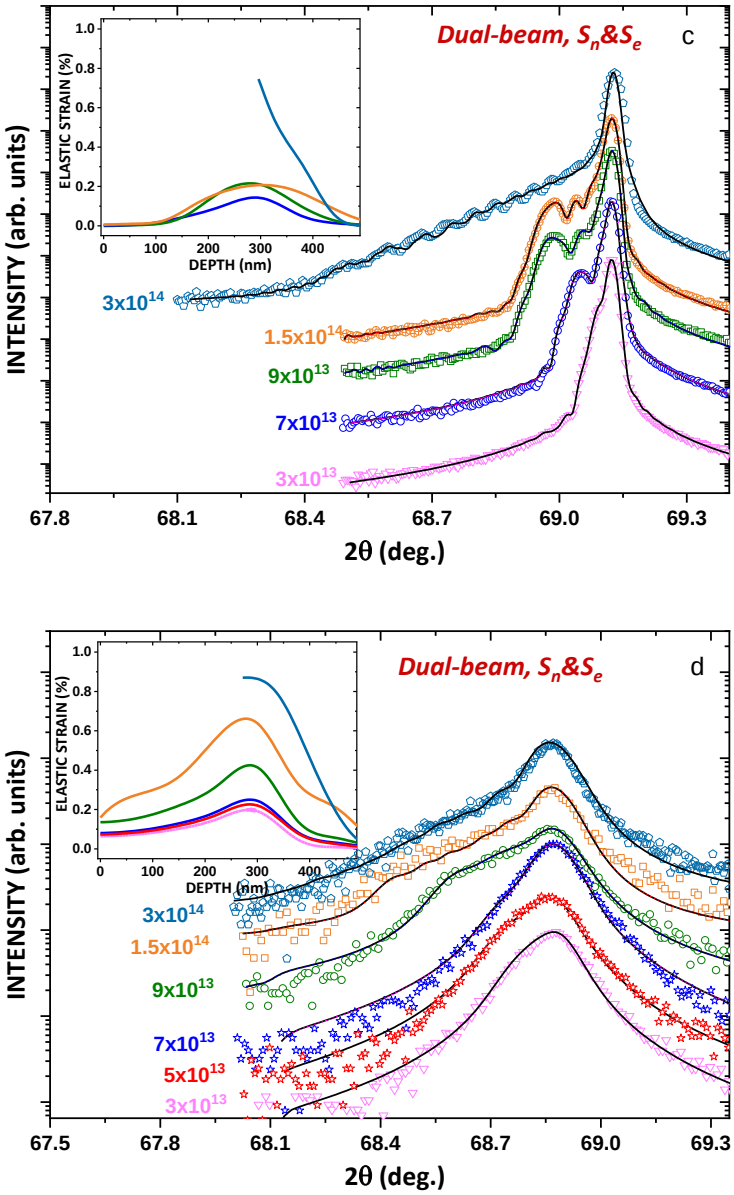

Figure 3

XRD signals around the (004) reflection recorded on Si-b (a,c) and Si-tl (b,d). Figures a and b correspond to samples irradiated with 900 keV I ions only (S_n), while figures c and d refer to crystals irradiated with both 900 keV I ions and 27 MeV Fe ions (S_n&S_e). Experimental data are represented by symbols and solid lines are best fits to those data obtained with the RaDMaX-Online program [27]. Fluences (in cm^{-2}) are given next to each curve. In insets are displayed the elastic-strain depth profiles derived from the fits with RaDMaX.

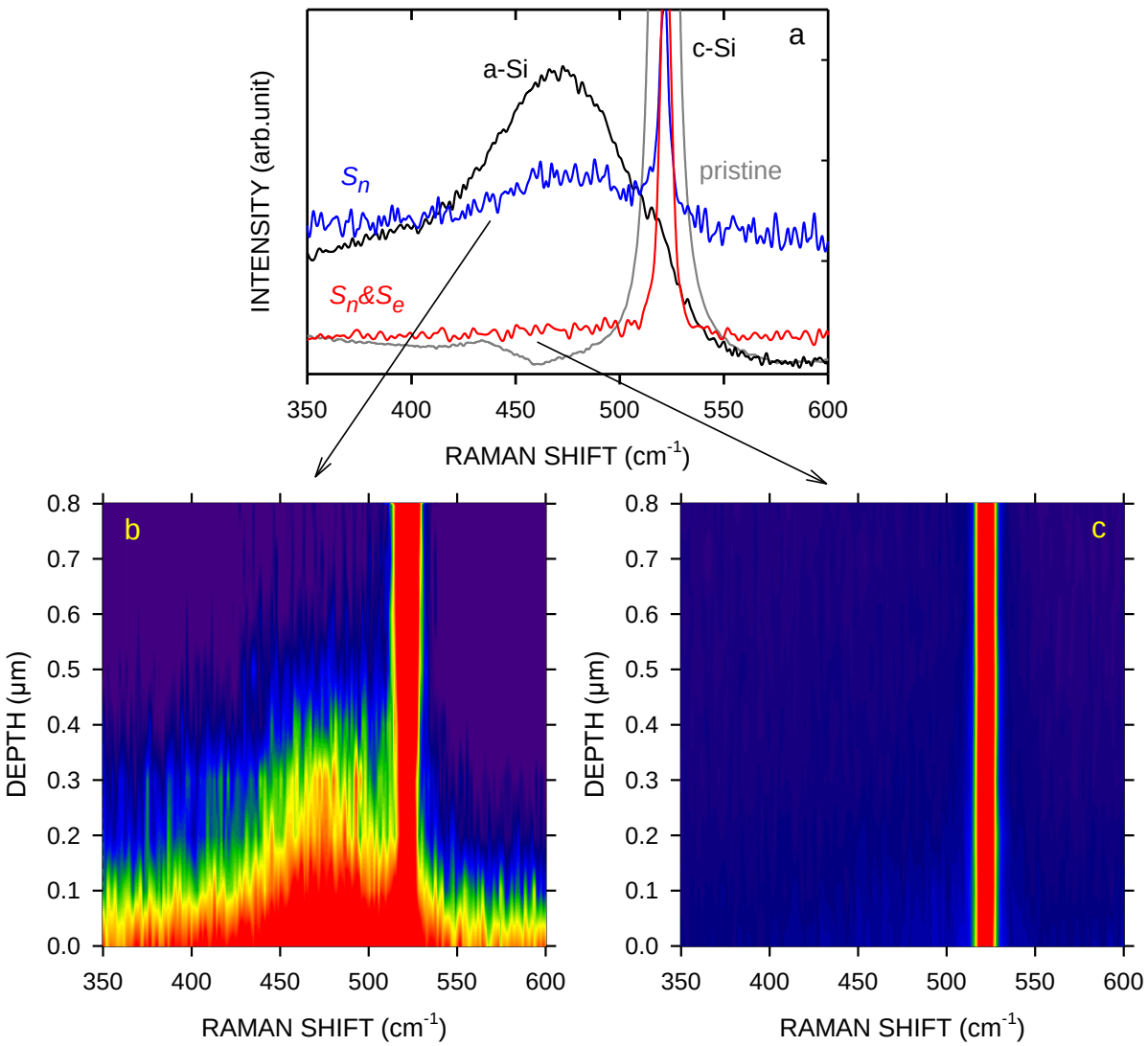

Figure 4

(a) Raman spectra recorded on a Si single crystal. Gray line: pristine sample; black line: amorphous sample; blue line: crystal irradiated with 900 keV I ions (S_n); red line: crystal simultaneously irradiated with a dual 900 keV I and 27 MeV Fe ion beam (S_n&S_e).

(b) Raman map recorded on a cross-section of a Si single crystal irradiated with 900 keV I ions. Note that the color scale goes from the less intense (blue) to the most intense (red) signals.

(c) Raman map recorded on a cross-section of a Si single crystal simultaneously irradiated with a dual 900 keV I and 27 MeV Fe ion beam.

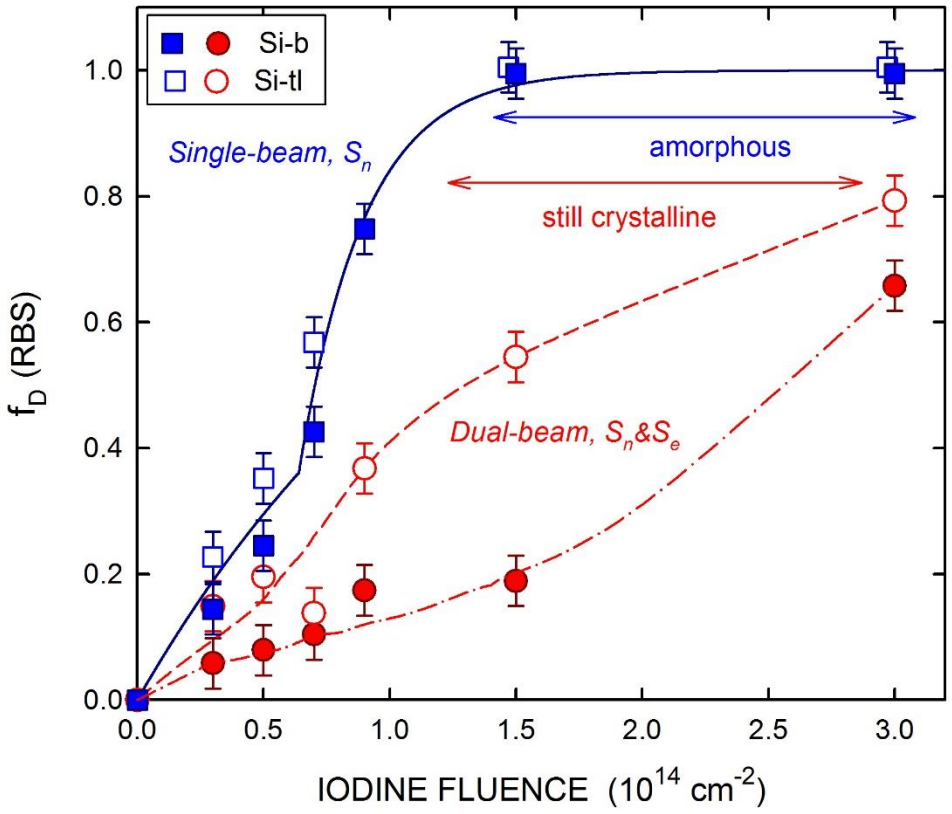

Figure 5

Damage fraction (f_D) vs iodine fluence, measured by RBS/C on Si-b (filled symbols) and Si-tl (open symbols) irradiated at RT either with 900 keV I ions alone (blue squares) or simultaneously with 900 keV I ions and 27 MeV Fe ions (red circles). The solid blue line is a fit to RBS/C data using a multi-step damage accumulation model [31]; dashed and dashed-dotted red lines are drawn for visualization purposes.

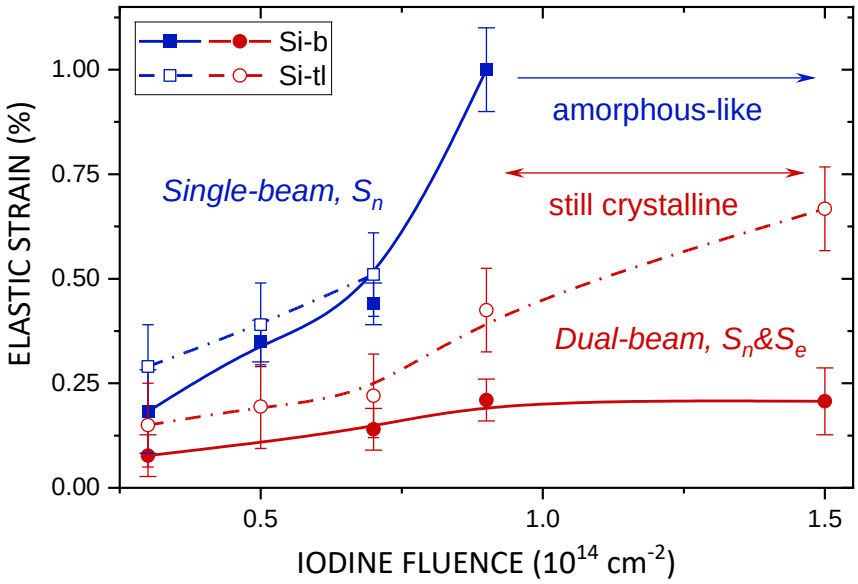

Figure 6

Elastic strain vs iodine fluence, measured by XRD on Si-b (filled symbols) and Si-tl (open symbols) irradiated at RT either with 900 keV I ions alone (blue squares) or simultaneously with 900 keV I ions and 27 MeV Fe ions (red circles). Solid and dashed lines are drawn for visualization purposes.